related to WPEC subgr 16 IEC-148

EFFECTS OF SHAPE DIFFERENCES IN THE LEVEL DENSITIES OF THREE FORMALISMS ON CALCULATED CROSS SECTIONS

C. Y. Fu
Oak Ridge National Laboratory, Oak Ridge, TN, USA

ABSTRACT

Effects of shape differences in the level densities of three formalisms on calculated cross sections and particle emission spectra are described. Reactions for incident neutrons up to 20 MeV on ^{58}Ni are chosen for illustrations. Level-density parameters for one of the formalisms are determined from the available neutron resonance data for one residual nuclide in the binary channels and from fitting the measured (n, n'), (n, p), and (n, α) cross sections for the other two residual nuclides. Level-density parameters for the other two formalisms are determined such that they yield the same values as the above one at two selected energies. This procedure forces the level densities from the three formalisms used for the binary part of the calculation to be as close as possible. The remaining differences are in their energy dependences (shapes). It is shown that these shape differences alone are enough to cause the calculated cross sections and particle emission spectra to be different by up to 60%.

1. INTRODUCTION

The evaluated ^{58}Ni(n, α) cross sections in the EFF-2 (European), ENDF/B-VI (U. S.), and JENDL-3 (Japanese) libraries are shown in Fig. 1. The resolution of the large differences between EFF-2 and ENDF/B-VI was the planned contribution for the first year of this Coordinated Research Program (CRP). It was found that most of these differences are due to factor-of-3 differences in the level densities used in the calculations performed for the evaluations. At the time these evaluations were being carried out, few data were available for this cross section, hence the heavy dependence on calculation. This part of the work has been reported in detail elsewhere[1] and is summarized in Section 2.

For the second year of the CRP, the level-density shape differences between Gilbert-Cameron[2] (G-C) and Back-Shifted Fermi Gas[3] (BSFG) were studied via calculated cross sections and particle emission spectra for ^{58}Ni for incident neutrons up to 20 MeV. Parameters for G-C were taken from the above work and those for BSFG were determined such that the resulting level densities agree with G-C at the top of the discrete-level region and near the neutron binding energy for ^{58}Ni, ^{58}Co, and ^{55}Fe. This procedure forces the level densities from the two formalisms to be as close as possible for the binary part of the calculation. The remaining differences are in the shapes of the two formalisms that, as shown in Section 3, are capable of causing the calculated cross sections and particle emission spectra to be different by up to 60%.

For the final year of this CRP, the Generalized Super-fluid Model[4] (GSM) was added to the TNG code[5] as a third level-density option. Again the shape effects were studied

via ^{58}Ni. However, this time the calculations started with a new evaluation for the s-wave level spacing, D_0, for ^{55}Fe. The Fermi gas parameter a corresponding to this D_0 in the G-C formalism was determined using the G-C pairing correction and a standard formula[4] for the spin cutoff parameter. The parameters for the constant temperature part of G-C were determined automatically in TNG. Since the D_0's for ^{58}Ni and ^{58}Co are not known experimentally, the corresponding a's in the G-C formalism were found in a series of TNG calculations to fit approximately the (n,n'), (n,p), and (n,α) cross-section data. Several new ^{58}Ni(n,α) data sets reported in the 1994 CRP meeting were taken into account in this fit. The parameters for BSFG and GSM were then obtained by forcing them to agree with G-C at two energies in the same manner as in Section 3 to study the shape effects of the three formalisms. The use of a smaller D_0 for ^{55}Fe resulted in larger values for a for all three residual nuclides, which led to different (n,α) cross-section shapes between G-C and BSFG than those obtained in in Section 3. The cross-section ratios and particle-emission spectral ratios between GSM and G-C are markedly different from those between BSFG and G-C. This part of work is described in Section 4.

2. EFF-2 and ENDF/B-VI

It is seen in the evaluated ^{58}Ni(n,α) cross sections shown in Fig. 1 that ENDF/B-VI is larger than EFF-2 up to 18 MeV and is about twice as large at 8 MeV. In addition, EFF-2 has a rise-flatten-rise shape not seen in ENDF/B-VI. The resolution of these differences required complete understanding of the formulas and parameters used in the two calculations.

The calculation for EFF-2 was done by Mario Uhl using his MAURINA code[6] and the calculation for ENDF/B-VI was performed by Dave Hetrick with TNG. The two codes use different pre-equilibrium models and different level-density formalisms. Discussion of this problem with Uhl led to the conclusion that one should at first concentrate in the 4 to 12 MeV region where the discrepancy is the largest and where there is a shape change in the cross sections. In this energy region the pre-equilibrium and tertiary-reaction complications can be avoided while the differences in the level-density formalisms are being studied. For these reasons, the present conclusions should be valid only below 12 MeV but the results presented between 12 and 20 MeV are still rather clear and helpful. Because the problems are being solved using the same code, isolation of the effects of each model parameter is possible.

During the presentation of this problem at a NEANSC meeting on international evaluation cooperation, Herbert Vonach suggested that using larger level density for the (n,n') channel in Hetrick's calculation would depress the calculated (n,α) cross section near 8 MeV. This observation is examined quantitatively as described below.

Hetrick's calculation was reviewed first. It turned out that his calculated (n,α) cross sections are 20% larger near 8 MeV than shown in Fig. 1. He reduced the calculated results between 6 and 10 MeV to agree with the data measured by Qaim[7]. During this time, Vonach sent information for discrete levels of ^{58}Ni, showing that the level density used for the (n,n') channel in Hetrick's calculation should go higher. This new level scheme was adopted and led to higher level densities between 4 and 10 MeV. This higher level density for the (n,n') channel, however, disrupted the good fits to the (n,n') and (n,p)

cross-section data achieved by Hetrick. To restore the good fits, minor adjustments in the level-density parameters for ^{58}Ni and ^{58}Co were made. These adjustments resulted in (n,α) cross sections slightly smaller than those of ENDF/B-VI shown in Fig. 1. So the problem was hardly solved. However, a complete understanding of the TNG calculation was established as a basis for comparison with Uhl's results. The revised calculation is referred to below as Fu's calculation. The new G-C parameters used are listed in Table 1 where U_0 is the G-C pairing correction. The differences between Fu's calculation and Uhl's represent the true calculational differences between ENDF/B-VI and EFF-2 shown in Fig. 1.

When Uhl was performing the evaluation, he was not aware of the data of Qaim[7,8] shown in Fig. 1. However, he knew about the 14.8-MeV measurement of Grimes et al.[9] (not shown in Fig. 1). His calculated (n,α) cross sections passed through Grimes et al. data and were therefore adopted for EFF-2.

All inputs Uhl used in MAURINA were tried in TNG to see if the EFF-2 cross section shown in Fig. 1 could be reproduced. To achieve this, however, the BSFG level-density formalism, used in MAURINA, had to be added to TNG as an option. And a special version of TNG was created to accommodate the energy-dependent radii used in the optical model of MAURINA. Uhl's results as shown in Fig. 1 were reproduced to about 10%. The remaining 10% difference could be due to other code differences, such as treatment of widths fluctuations. By testing each model parameter individually, its effect on the calculated (n,α) cross sections was isolated. The level-density differences in the three binary channels between the two calculations account for about 80% of the (n,α) cross-section differences, as explained in the following paragraph. The differences in the optical-model parameters account for the rest.

The level densities used in Uhl's and Fu's calculations for ^{58}Ni, ^{58}Co, and ^{55}Fe are compared as ratios in Fig. 2. The BSFG parameters used by Uhl are also listed in Table 1 to compare with the G-C parameters used in Fu's calculation. The symbol δ in Table 1 represents the sum of a pairing correction and a back energy shift. As shown in Table 2 for an incident neutron energy of 8 MeV, more outgoing neutrons and protons reach the level-density regions (continuum) than the corresponding discrete regions, while the alpha-particles reach mainly the discrete levels. Higher level densities in ^{58}Ni and ^{58}Co in Uhl's calculation increase the continuum (n,n') and (n,p) cross sections at the expense of the discrete (n,α) cross section. This explains the smaller and flattened (n,α) cross sections in EFF-2 between 6 and 10 MeV. As incident neutron energies go higher than 10 MeV, most outgoing alpha-particles begin to see the large ^{55}Fe level densities in Uhl's calculation, and the (n,α) cross section rises again. Note that the "Uhl's calculation" here represents a TNG calculation using all of Uhl's parameters.

The changes in proportions of the discrete and continuum cross sections between the two calculations seen in Table 2 also cause changes in the particle emission spectra for an incident energy of 8 MeV.

The calculation for JENDL-3 shown in Fig. 1 was performed by S. Iijima. Communication with him ended in December 1989 when he died. Therefore, a detailed examination of his calculation was not possible.

During the course of this part of work, it became obvious that there is a large shape difference between the level densities of BSFG and G-C. A first attempt to isolate the

effects of these shape differences on calculated cross sections and particle emission spectra is presented in the next section.

3. SHAPE DIFFERENCES BETWEEN BSFG and G-C

For this part of study, the cross sections and particle emission spectra in Fu's calculation above were chosen as the G-C reference. This choice is simply a matter of convenience because the numerical results have been stored. A more intelligent choice, leading to higher level densities, is described in Section 4. However, the present results remain interesting, particularly in light of the new results to be presented in Section 4.

The BSFG parameters for each binary residual nuclide were determined by fitting the BSFG level densities to those of G-C at the top of the discrete region, E_c, and the tangent point, E_x, separating the Fermi-gas part and the constant-temperature part of G-C. The resulting BSFG parameters are listed in Table 1. The level-density ratios BSFG/G-C up to 14 MeV are shown in Fig. 3. The corresponding particle emission spectra ratios for 14-MeV incident neutrons are shown in Fig. 4.

The a parameters labeled 'BSFG fitted to G-C' are some 16% smaller than those used in Uhl's calculation. For ^{58}Ni and ^{55}Fe, there are increased back shifts. Both factors contribute to the factor-of-3 level density-density ratios labeled Uhl/Fu in Fig. 2.

It was decided to adopt E_x instead of the neutron binding energy as one of the fitting energies because E_x is fairly close to the neutron binding energy and has the additional advantage of representing a point of characteristic change in the shape of the G-C level densities. Below E_x, where BSFG level densities are always higher than G-C, the ratios shown in Fig. 3 represent the ratios between level densities having a Fermi-gas and a constant-temperature shape. Above E_x, BSFG and G-C are two Fermi gases with different energy shifts, so must have different a's to yield the same level densities at E_x. In the present case, the a's in BSFG are less than in G-C, so the BSFG/G-C ratios above E_x decrease with increasing excitaion energy.

In Fig. 4, the neutron, proton, and alpha-particle emission ratios above 2 MeV are essentially due to binary reactions and show peaks roughly corresponding to the level-density peaks seen in Fig. 3, shifted to higher energies for protons and alpha-particles by the respective threshold. The ratios for emitted neutrons less than 2 MeV is smaller than unity because the (n,pn) contribution in BSFG is smaller.

The level-density ratios up to 20 MeV and particle-emission ratios for 20-MeV incident neutrons are shown respectively in Figs. 5 and 6. The differences seen in Figs. 3 and 4 are now magnified. The only complication due to tertiary reactions is in the neutron emission ratios for which the peak seen in Fig. 4 is missing because the low energy region is filled by tertiary-reaction contributions, especially (n,pn).

The (n,α) cross sections calculated using BSFG and G-C are compared in Fig. 7. The agreement is nearly perfect up to 10 MeV, above which the two results start to diverge. There is no rise-flatten-rise shape around 8 MeV in the BSFG calculation because the BSFG level densities are now much lower and the differences between BSFG and G-C are only 10% of those seen in Fig. 2. The relative changes between the discrete and continuum cross sections, listed in Table 2, are rather close to those of the G-C calculation, meaning the particle emission spectra between the two calculations also agree. However, this is only

a special case. As shown below in Section 4, the rise-flatten-rise shape in BSFG re-appears when a set of larger level densities is used.

The (n,α) cross sections in Fig. 7 show that BSFG at 20 MeV is 60% larger than G-C. In the BSFG calculation at this energy, most outgoing alpha-particles see larger level densities than outgoing neutrons and protons do (see Fig. 5) because of the higher Coulomb energy and lower threshold for alpha-particle emission.

The importance of the level density problem on theoretical computation of (n,α) cross sections and alpha-particle emission spectra is now well established. But many questions remain. In the following, a more thorough investigation is carried out which, as pointed out in the concluding remarks, is still inadequate to fully clear up the problems associated with G-C, BSFG, and GSM.

4. ADDITIONAL ANALYSES AND INCLUSION OF GSM

A new calculation for the ^{58}Ni cross sections was made (1) to account for a new evaluation of s-wave level spacing D_0 for ^{55}Fe, (2) to account for (n,α) cross sections measured for this CRP, and (3) to get a better set of G-C level-density parameters for ^{58}Ni, ^{58}Co, and ^{55}Fe that yield reasonable agreement with the available (n,n'), (n,p), and (n,α) cross-section data, to begin the investigation with.

a. D_0 for ^{55}Fe

Among the level densities required for calculating the binary cross sections, the only measured D_0 available is for ^{55}Fe. This D_0 value was fixed at 14.4 keV (20.4 keV in the G-C calculations above) based on the recent analysis of Zhao and Su[10]. The Fermi-gas parameter a in G-C was derived from D_0 using:

$$U = E - U_0, U = at^2, \sigma^2 = (6/\pi^2)a\langle m^2\rangle t, \langle m^2\rangle = 0.24A^{2/3},$$

where E is the excitation energy and U_0 is the pairing energy correction, taken here as 1.54 MeV.

In the TNG code, the required input for G-C are a, $\langle m^2\rangle$, and U_0 for the Fermi gas part. The parameters for the constant temperature part of G-C (energy shift E_0, temperature T, and tangential point E_x) are determined automatically in TNG from the input for the Fermi gas part and the discrete levels. The energy of the highest discrete level is called E_c. If $\langle m^2\rangle$ is not given, TNG takes the formula above as default. So in the calculations using G-C, the necessary input are a and U_0 while the adjustable one to fit cross sections is normally only a.

The effective excitation energy U is defined differently in the BSFG and the GSM formulas to be given below.

b. Fit to ^{58}Ni cross sections

The a values for ^{58}Ni and ^{58}Co were adjusted via a series of TNG calculations to fit (n,n'), (n,p), and (n,α) cross sections using G-C. Since no other model parameters were adjusted, the fit is not optimal. However, it is important to note that once the a value for ^{55}Fe is fixed, there can only be one set of a's possible in the fit.

The resulting G-C parameters are shown in Table 3, where the BSFG and GSM parameters described below are also listed for comparison.

The resulting cross sections are shown in Fig. 8. Experimental cross sections are not shown, but it is sufficient for the present purpose to note that the calculated values agree with 'evaluated' data to about 10%.

c. BSFG VERSUS G-C

The BSFG a and the shift Δ for each of the binary residual nuclides are obtained by fitting the BSFG level densities to G-C determined above at E_c and E_x. The resulting BSFG parameters can also be found in Table 3.

The BSFG/G-C ratios up to 20 MeV are shown in Fig. 9. Note each E_x is now smaller and closer, compared to that in Fig. 5, to the neutron binding energy due to the use of a larger a. This set of smaller E_x drops the BSFG/G-C ratios above E_x some more. The relative changes in the BSFG/G-C ratios among the three residual nuclides are different and result in different changes in the cross sections.

The spin cutoff factor in BSFG used here is given by

$$\sigma^2 = 0.0150A^{5/3}t, U - \Delta = at^2 - t$$

The effects of this different spin cutoff factor on cross sections and particle emission spectra have been determined to be much smaller than the shape effects being addressed in this report.

The effects of the level-density shape differences between BSFG and G-C on cross sections are shown in Fig. 10 and on particle emission spectra for an incident energy of 20 MeV are shown in Fig. 11.

From Fig. 10, it is seen that the BSFG/G-C ratios for (n,α) have a valley between 4 and 12 MeV. This means the rise-flatten-rise shape in EFF-2 seen in Fig. 1 but not seen in Fig. 7 re-appears. This phenomenon cannot be explained by comparing the differences in the BSFG/G-C ratios shown in Figs. 5 and 9. The explanation can be found from the larger a's used here that increase the continuum parts, relative to the discrete parts, of all cross sections (Table 4). Since the (n,n') and (n,p) cross sections at 8 MeV have much larger continuum components than (n,α), the preference for neutron and proton emission due to the larger BSFG level densities are magnified. For incident energies greater than 12 MeV, the outgoing alphas in the BSFG calculation begin to see larger BSFG level densities than the outgoing neutrons and protons do, so the BSFG (n,α) gets larger.

The particle emission spectra ratios shown in Fig. 11 have the same behavior as shown above in Fig. 6. For example, neutron emission below 4 MeV for BSFG is larger because the BSFG (n,pn), the dominant low-energy neutron emitter, is larger. And neutron emission around 10 MeV for BSFG is reduced because the BSFG (n,n') cross section is reduced.

In summary, the present set of larger a's yields a different shape in the BSFG (n,α) cross sections but the same shapes in the particle emission spectra compared to a lower set of a's used in Section 3.

d. GSM VERSUS G-C

The GSM asymptotic a and the shift δ for each of the binary residual nuclides are obtained by fitting GSM level densities to G-C determined above at E_c and E_x.

The resulting GSM/G-C level density ratios are shown in Fig. 12. These ratios are closer to unity than BSFG/G-C ratios shown in Fig. 9, due to the energy-dependent Fermi-gas parameters that increase with increasing excitation energy. However, the differences in cross sections and particle emission spectra between GSM and G-C are larger than between BSFG and G-C, as discussed below. The GSM parameters are also listed in Table 3. Values of the shell corrections needed for GSM were obtained from the HERMES code of Mengoni[11].

Note that the spin cutoff factor in GSM is the same as used above for G-C, but U is defined differently:

$$U = E - E_{cond} + n\Delta_0 + \delta, \Delta_0 = 12A^{-1/2}$$

where A is the mass number, n = 0, 1, 2 for even-even, odd-A, and odd-odd nuclide. E_{cond} is the condensation energy in the model calculated from other input parameters. $E_{cond} - n\Delta_0$ is the pairing correction. The effects of the level-density shape differences between GSM and G-C on cross sections are shown in Fig. 13 and on particle emission spectra for an incident energy of 20 MeV are shown in Fig. 14. The super-fluid region has no impact here because this region lies below E_c.

From Fig. 13, it is seen that the GSM/G-C ratios for (n, α) have a maximum at 8 MeV instead of a minimum seen in Fig. 10. This new behavior can be explained by comparing the level density ratios of Figs. 9 and 12, and at the same time, looking at the GSM distributions of discrete and continuum cross sections listed in Table 4. While for an incident neutron energy of 8 MeV all GSM level densities are greater then G-C, the distribution between the discrete and continuum cross sections have changed. The outgoing neutrons and protons in GSM see fewer continuum levels, resulting in smaller (n, n') and (n, p) continuum cross sections and larger (n, α) discrete and continuum cross sections. In other words, the 8-MeV maximum in the GSM/G-C is more a result of redistribution of cross section within the GSM calculation itself than a difference between the level densities of GSM and G-C. For incident energies greater than 12 MeV, the GSM level densities clearly favor the (n, n') cross sections.

The shapes of the GSM/G-C ratios for particle emission shown in Fig. 14 are reversed from those of BSFG/G-C shown in Fig. 11. For example, neutrons emitted below 4 MeV in the GSM calculation are lower because the GSM (n, pn) cross sections are smaller. And neutron emissions for GSM around 10 MeV are higher due to larger GSM (n, n') cross sections.

Even though the GSM/G-C ratios are closer to unity than BSFG/G-C, the differences between calculated GSM and G-C cross sections and particle emission spectra are larger due to the larger relative changes in level densities among the three residual nuclides. For example, between 10 and 20 MeV, BSFG/G-C ratios in Fig. 9 move down with energy but stay parallel. This fact changes the particle emission spectra more than the cross sections. On the other hand and in the same energy range, the GSM/G-C ratios in Fig. 12 also decrease with energy but do not stay parallel. This new behavior changes the cross

sections more and changes the particle emission spectra by an even larger amount because the differences in cross sections also show up in the emission spectra.

5. CONCLUDING REMARKS

It is now clear that, given a nucleus with adequate number of discrete levels and neutron resonance data, the three level-density formalisms studied in this report would give different level densities at all excitation energies other than at the top of the discrete-level region and the neutron binding energy. The resulting calculated cross sections, particularly (n,α), and particle emission spectra would also be different by up to 60%. In less ideal situations where little or no experimental level-density data exist, the calculated (n,α) cross sections can differ by a factor of 2 due to the additional uncertainty in the level-density parameters.

In this section, tentative remarks, based on theoretical consideration, on the strengths and weaknesses of each level-density model studied in this report are offered for the sake of stimulating wider research in this important area.

The fact that G-C has a constant temperature part for low excitation energies and a Fermi gas part for higher energies is a strength, not a weakness as generally perceived[3,4], at least for the present calculations. First, the number of discrete levels in each residual nuclide required in the present calculations defines the level density at E_c rather well. Therefore the constant temperature part of G-C requires no input parameters. Second, the Fermi gas part used to fit the experimental D_0 value is not disrupted by an arbitrary energy shift (other than the pairing energy shift) that has no physical meaning in the Fermi gas model. The original argument by G-C for introducing the constant temperature part is to compensate for the low-energy collective levels not included in the Fermi gas model.

The weakness of G-C is in its shell correction that is included in a constant a for all excitation energies. At high excitation energies, in which particles far below the Fermi surface get excited, the shell correction should diminish. This dwindling shell correction is treated in GSM, one of its strengths.

GSM has the strongest physics in both pairing corrections and shell corrections. However, the fact that GSM still needs an arbitrary energy shift δ to fit both D_0 at the neutron binding energy and the level density in the discrete level region, at least for ^{55}Fe considered here, is a disappointment. It is seen from Fig. 12 that GSM/G-C is smaller than unity above E_x. This means the effects of the shift factor overpower the effects of the dwindling shell corrections. In case the shift factor is small, such as for ^{116}Sn in Ref. 4, the basic physics intended for GSM is maintained.

For similar reasons, the back shift Δ used in BSFG has no physical basis. Like G-C, the shell corrections in BSFG are accounted for in a constant a determined at the neutron binding energy, a second weakness.

As tentative recommendations, BSFG should be restricted to calculations at low energies, perhaps lower than 14 MeV. G-C may be used to much higher energies if shell corrections are small. For example, G-C should not be used for the Pb isotopes, probably not above 10 MeV, because of large shell corrections. GSM is not widely understood and deserves more applications to clear up any possible problems. In case the shift factor used in GSM is large, as in the present calculations for ^{58}Ni, the effects of the shift tend

to overpower the intended physics built in the super-fluid pairing model and the energy-dependent shell correction. And the required input of shell corrections for GSM from different sources[11,12] may be different.

6. ACKNOWLEDGMENTS

The work was sponsored by Office of Energy Research, Division of Nuclear Physics, U. S. Department of Energy, under contract DE-AC05-84OR21400 with Lockheed Martin Energy Systems, Inc.

7. REFERENCES

1. C. Y. Fu, D. C. Larson, D. M. Hetrick, H. Vonach, J. Kopecky, S. Iijima, Y. Yamamuro, T. Asami, S. Chiba, G. Maino, I. Mengoni, "Report of Subgroup 1 of the NEANSC Working Party on International Evaluation Cooperation," to be published by NEA Nuclear Data Bank.
2. A. Gilbert and A. G. W. Cameron, *Can. J. Phys.* **13**, 1446 (1965).
3. W. Dilg, W. Schantl, H. Vonach, and M. Uhl, *Nucl. Phys.* **A217**, 269 (1973).
4. A. V. Ignatyuk, J. L. Weil, S. Raman, and S. Kahane, *Phys. Rev.* **C47**, 1504 (1993).
5. K. Shibata and C. Y. Fu, "Recent Improvements of the TNG Statistical Model Code," ORNL/TM-10093 (1986), and C. Y. Fu, "A Consistent Nuclear Model for Compound and Precompound Reaction Cross-Section Calculations," ORNL/TM-7042 (1980).
6. M. Uhl, Institute of Radiation and Nuclear Phisics, University of Vienna, Vienna, Austria, private communication (1990).
7. S. M. Qaim, R. Wolfe, N. M. Rahman, *Nucl. Sci. Eng.* **88**, 143 (1984).
8. S. M. Qaim and N. I. Molla, *Nucl. Phys.* **A283**, 269 (1977).
9. S. M. Grimes et al., *Phys. Rev.* **C19**, 2127 (1979).
10. Z. Zhao and Z. Su, Chinese Nuclear Data Center, private communication (1994).
11. A. Mengoni and Y. Nakajima, *J. Nucl. Sci. Tech.* **31**, 151 (1994) and private communication (1995).
12. A. Zelenetsky, Institute of Atomic Energetics, Obninsk, Russia, private communication (1995).

Table 1. Level-density parameters for Figs. 2 and 3

		Ni-58	Co-58	Fe-55
Gilbert-Cameron Fu's calculation G-C (Fu) For Figs. 2, 3	a	5.400	6.200	5.909
	U	2.470	0	1.540
Back-Shifted Fermi Gas Uhl's calculation For Fig. 2	a	5.517	6.061	5.821
	δ	0.104	-2.571	-0.700
BSFG fitted to G-C (Fu) at EC and EX For Fig. 3	a	4.600	5.260	5.000
	δ	-0.500	-2.600	-1.100

Table 2. Discrete and continuum parts of Ni-58 cross sections (mb) for an incident energy for 8 MeV calculated using level-density parameters of Table 1

	Discrete			Continuum		
	(n,n')	(n,p)	(n,a)	(n,n')	(n,p)	(n,a)
G-C (Fu)	341	181	72.2	536	391	11.2
BS (Uhl-TNG)	217	42	37.9	612	502	16.2
BS fitted to G-C	344	176	70.9	528	400	12.9

This table corresponds to Fig. 7. All model parameters other than level densities were chosen for and stayed fixed throughout this paper.

Table 3. Level-density parameters for Figs. 9 and 12

		Ni-58	Co-58	Fe-55
Gilbert-Cameron For Figs. 9, 12				
	a	6.200	7.300	7.256
	U	2.470	0	1.540
Back-Shifted Fermi Gas For Fig. 9				
	a	5.322	6.210	6.188
	δ	0.210	-1.910	-0.210
Generalized Super-fluid Model For Fig. 12				
asymptotic	a	6.496	7.266	7.576
	δ	2.680	1.468	1.530
shell corr.		-4.037	-2.318	-2.977

Table 4. Discrete and continuum parts of Ni-58 cross sections (mb) for an incident energy of 8 MeV calculated using level-density parameters of Table 3

	Discrete			Continuum		
	(n,n')	(n,p)	(n,a)	(n,n')	(n,p)	(n,a)
G-C	296	144	57.7	580	444	12.1
BS fitted to G-C	265	114	45.4	628	471	12.7
GSM fitted to G-C	371	171	69.3	503	395	17.2

This table corresponds to Figs. 8, 10 , and 13. All model parameters other than level densities were chosen for and stayed fixed throughout the paper.

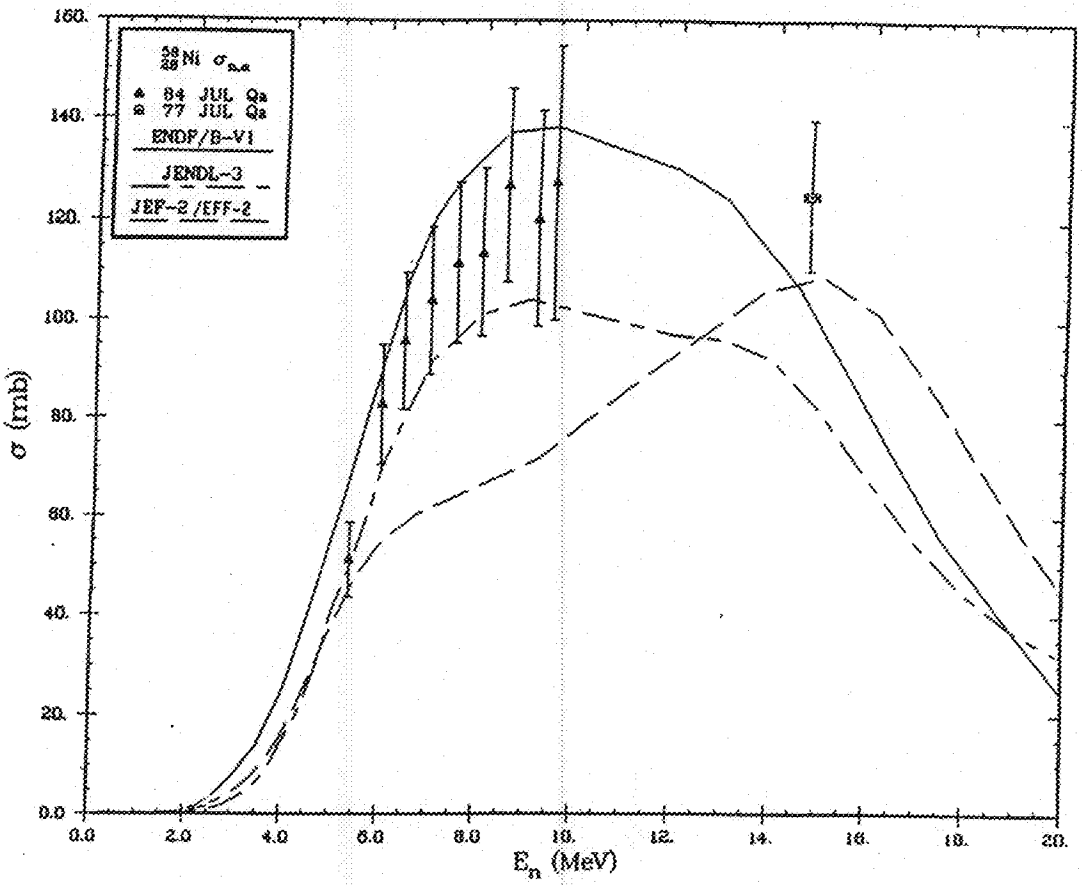

Fig. 1. Evaluated ^{58}Ni(n,α) cross sections in ENDF/B-VI, JENDL-3, and EFF-2. ENDF/B-VI at 8 MeV is twice as large as EFF-2, and EFF-2 has a rise-flatten-rise shape not seen in the other two evaluations. The data shown are due to Qaim et al[7,8].

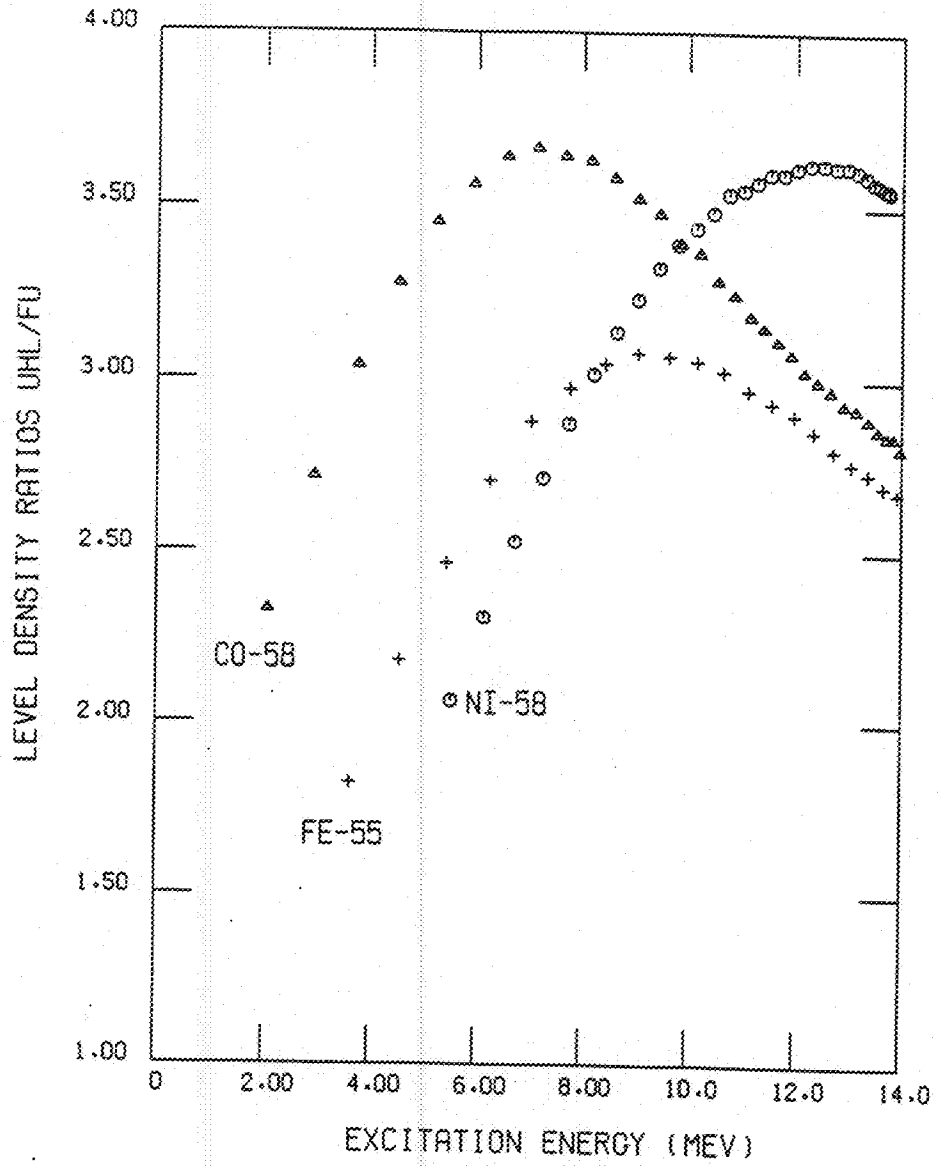

Fig. 2. Level densities used in Uhl's calculation for EFF-2 and in Fu's calculation (approximately representing ENDF/B-VI in Fig. 1) are compared as ratios for threee residual nuclides in the binary reactions of neutrons with ^{58}Ni. These level-density differences account for about 80% of the differences between the calculated ^{58}Ni(n,α) cross sections for ENDF/B-VI and EFF-2.

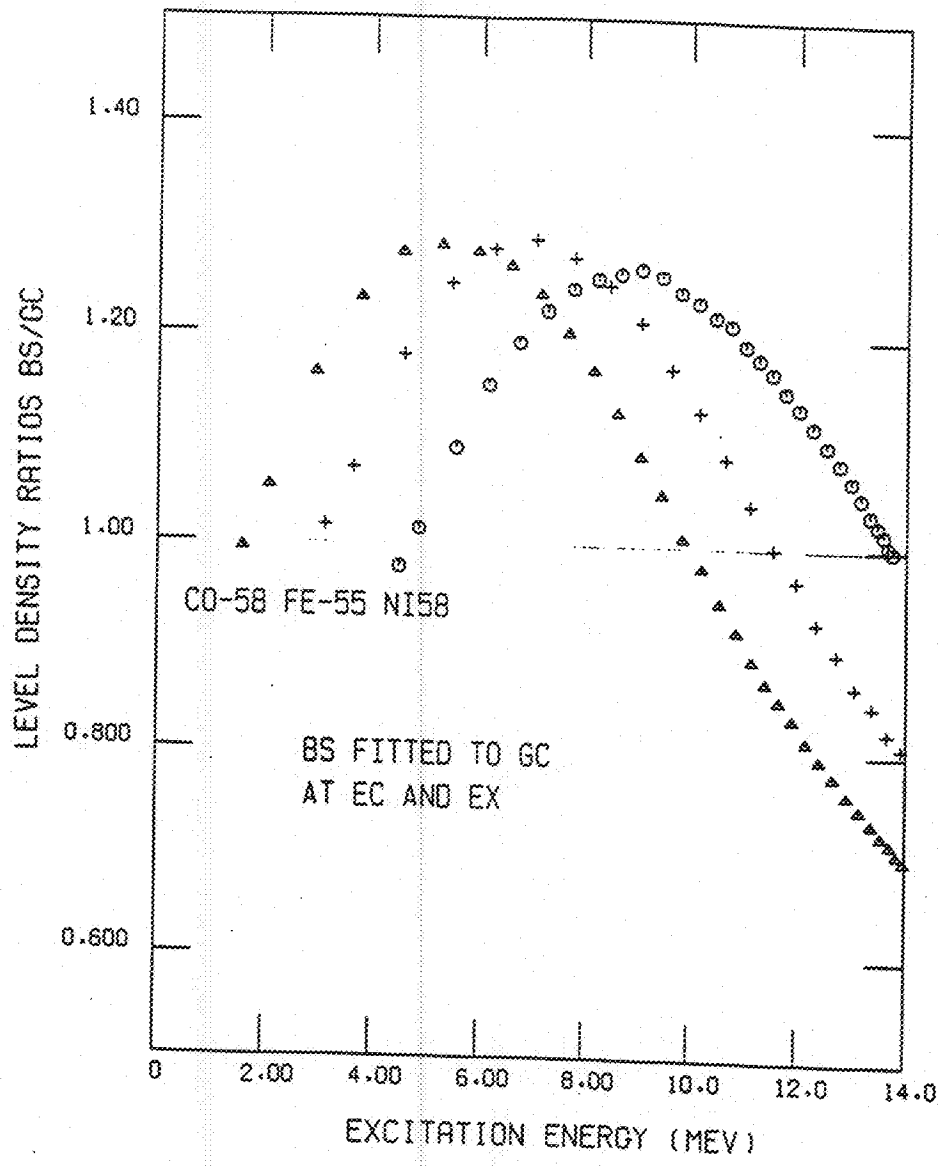

Fig. 3. Parameters of the BSFG formalism are determined by fitting its level densities at two energies, E_c and E_x, to G-C used in Fu's calculation shown in Fig. 2. The resulting level densities are compared as ratios for three residual nuclides in the binary reactions of neutrons with ^{58}Ni.

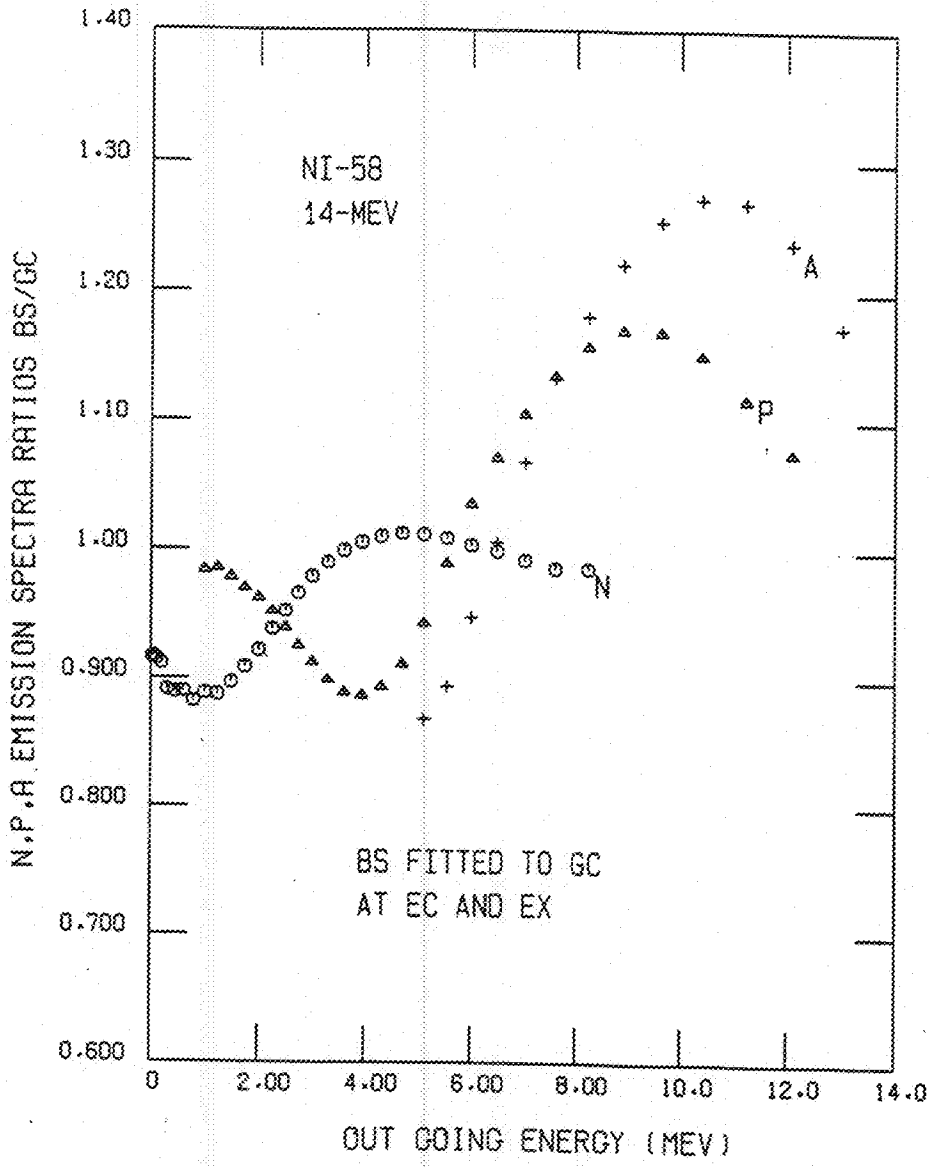

Fig. 4. Neutron, proton, and alpha-article emission spectra for an incident neutron energy of 14 MeV calculated using the BSFG and G-C level densities indicated in Fig. 3 are compared as ratios. The peaks in these ratios correspond to the peaks in the level-density ratios shown in Fig. 3, shifted by the respective reaction threshold.

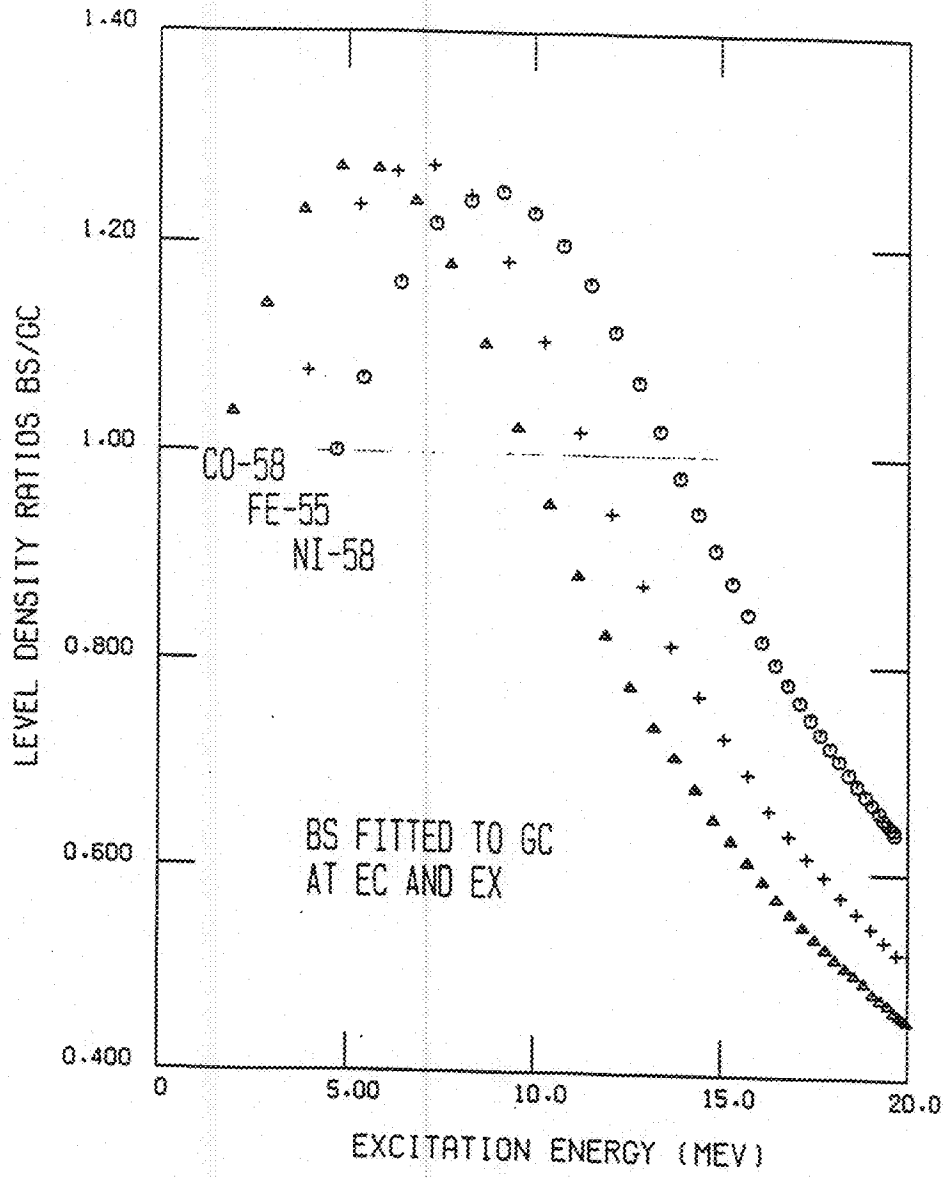

Fig. 5. Same as Fig. 3 but extended to higher excitation energies. The difference between BSFG and G-C level densities for each residual nuclide increases as the excitation energy increases above E_x.

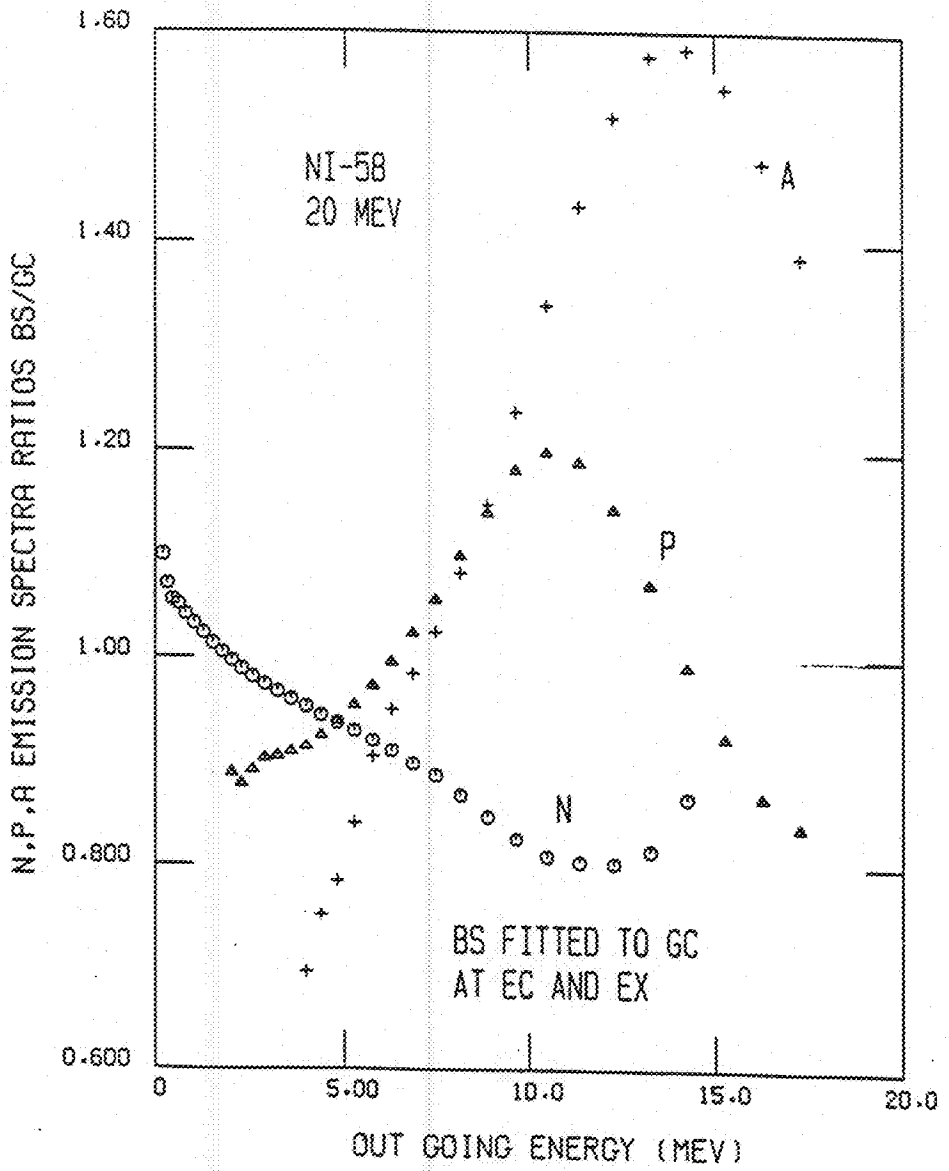

Fig. 6. Same as Fig. 4 but for an outgoing energy of 20 MeV. The differences between the calculated spectra are magnified, particularly for alpha-particles, from those for 14 MeV.

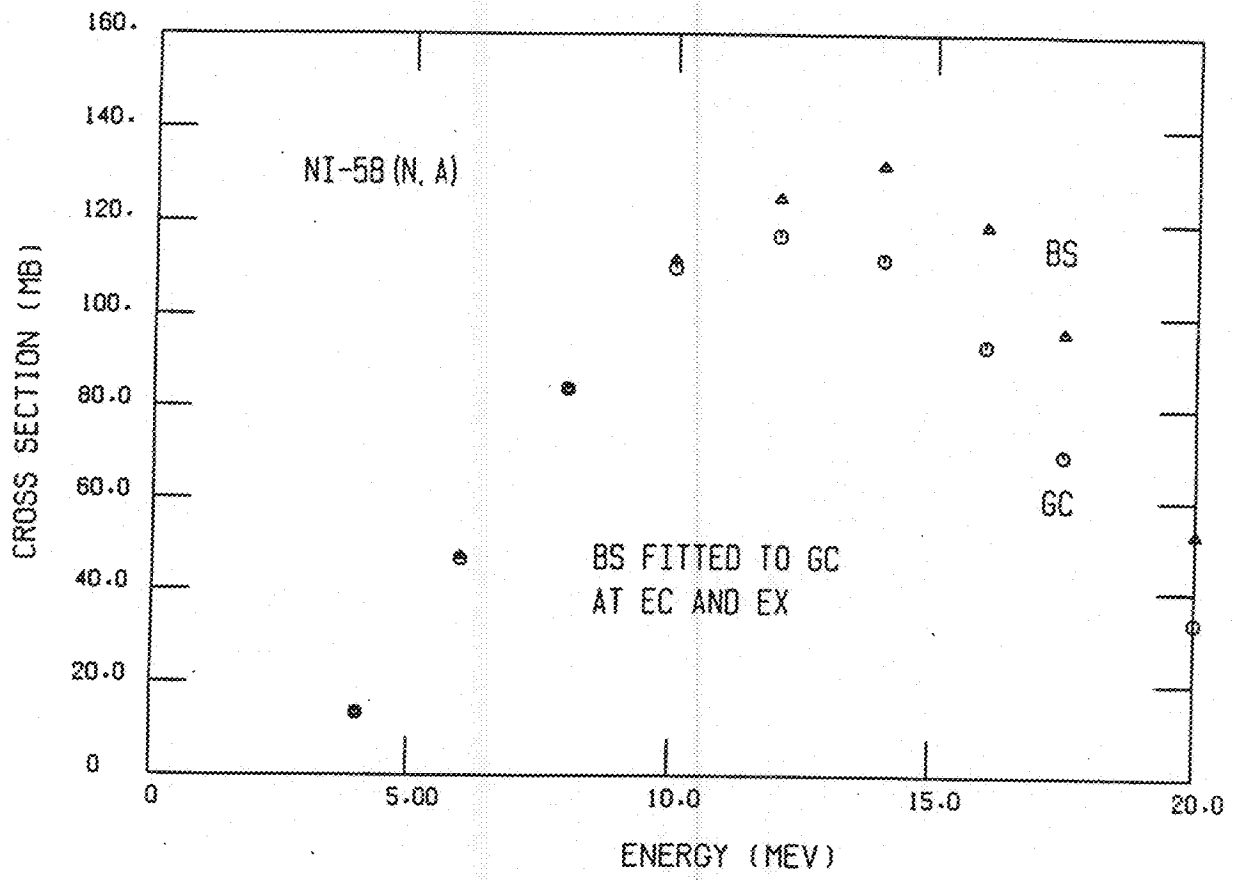

Fig. 7. The ^{58}Ni(n,α) cross sections calculated using BSFG and G-C shown in Fig. 5 are compared. At 20 MeV, BSFG is 60% larger than G-C. In BSFG calculation at this incident energy, most outgoing alpha-particles see larger level densities than outgoing neutrons and protons do because of the higher Coulomb energy and lower threshold for alpha-particle emission.

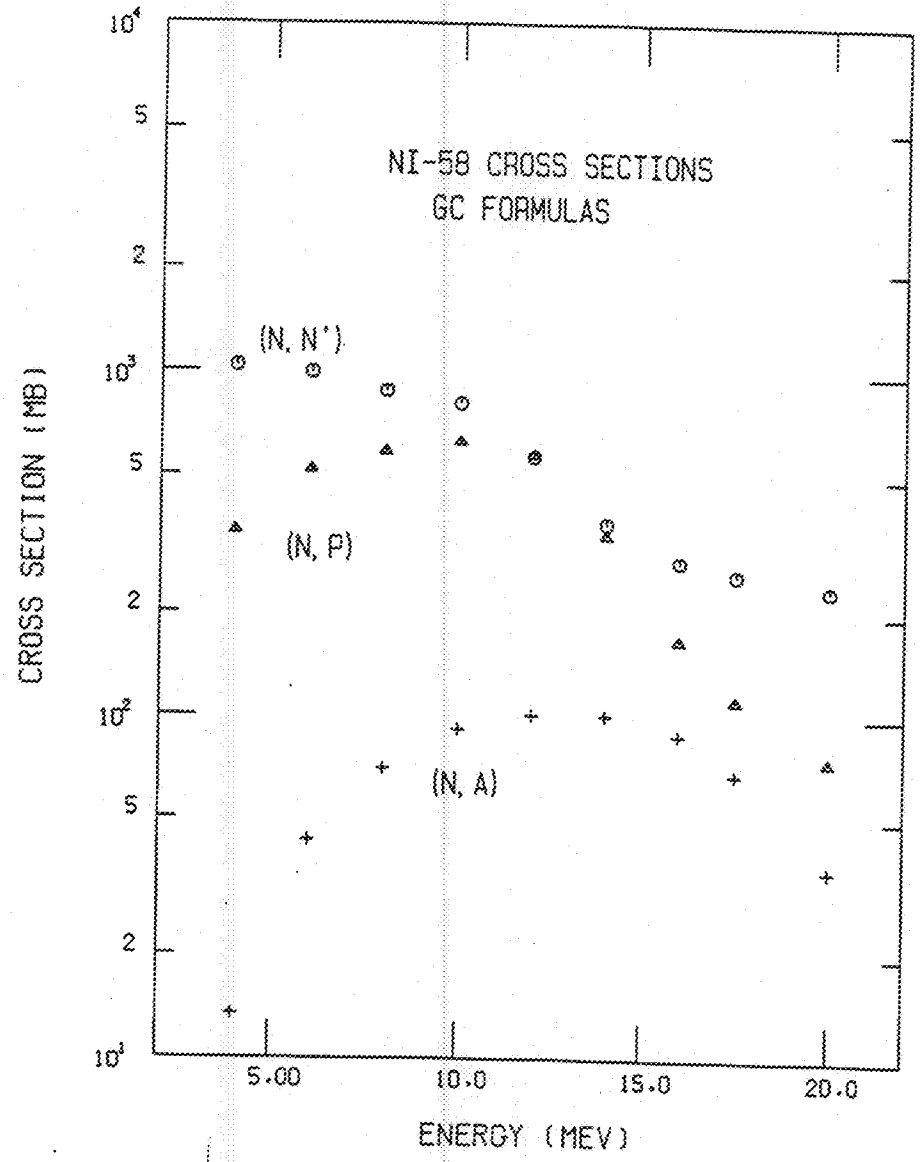

Fig. 8. ^{58}Ni(n,n'), (n,p), and (n,α) cross sections calculated using recommended level densities for the (n,α) channel and adjusted level densities for the (n,n') and (n,p) channels fitting the measured cross sections. This figure is presented as a basis for comparisons below.

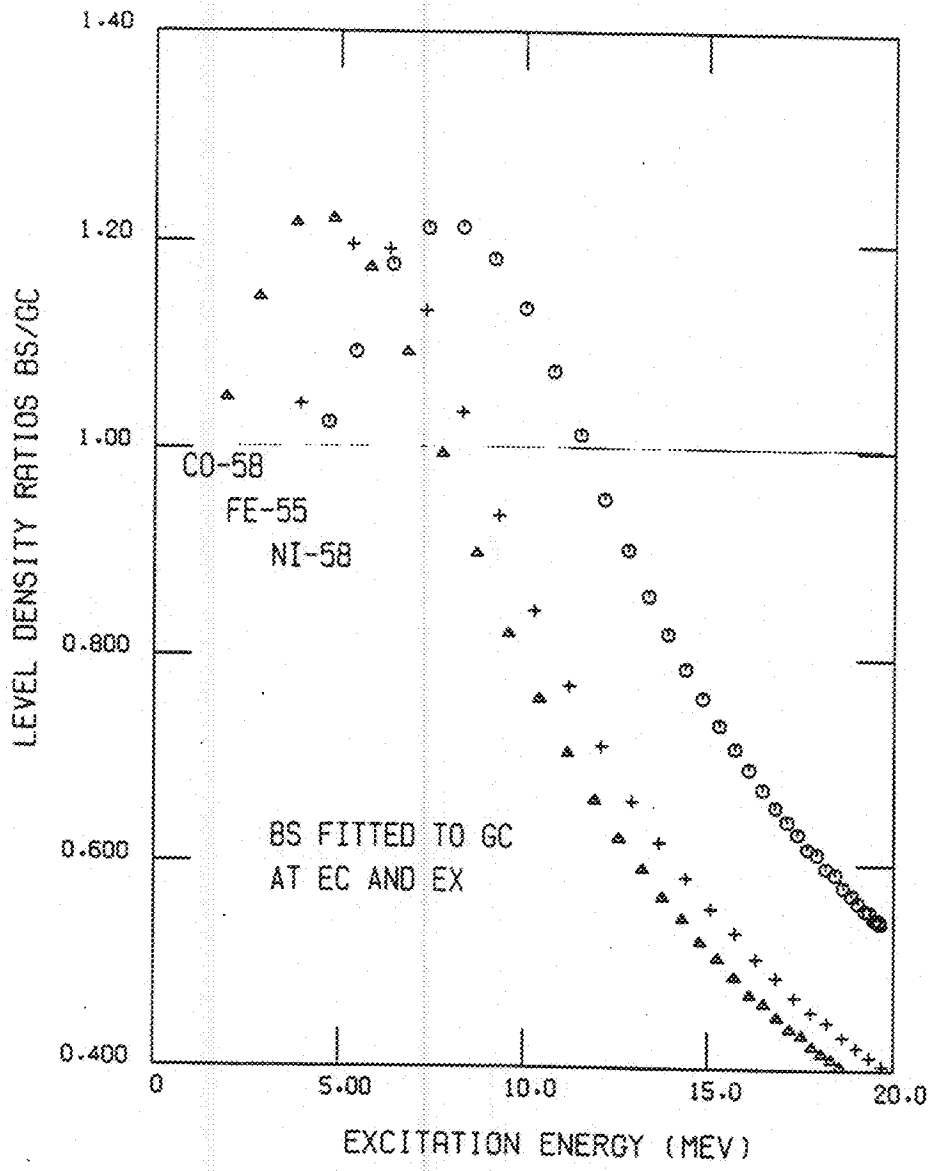

Fig. 9. Same as Fig. 5 except for a different set of level-density parameters obtained from the calculations shown in Fig. 8. Note the following differences from Fig. 5: the peak in ^{55}Fe ratios is lower, the E_x's are lower, the high-energy tails move down more, and the ^{55}Fe tail moves closer to ^{58}Co.

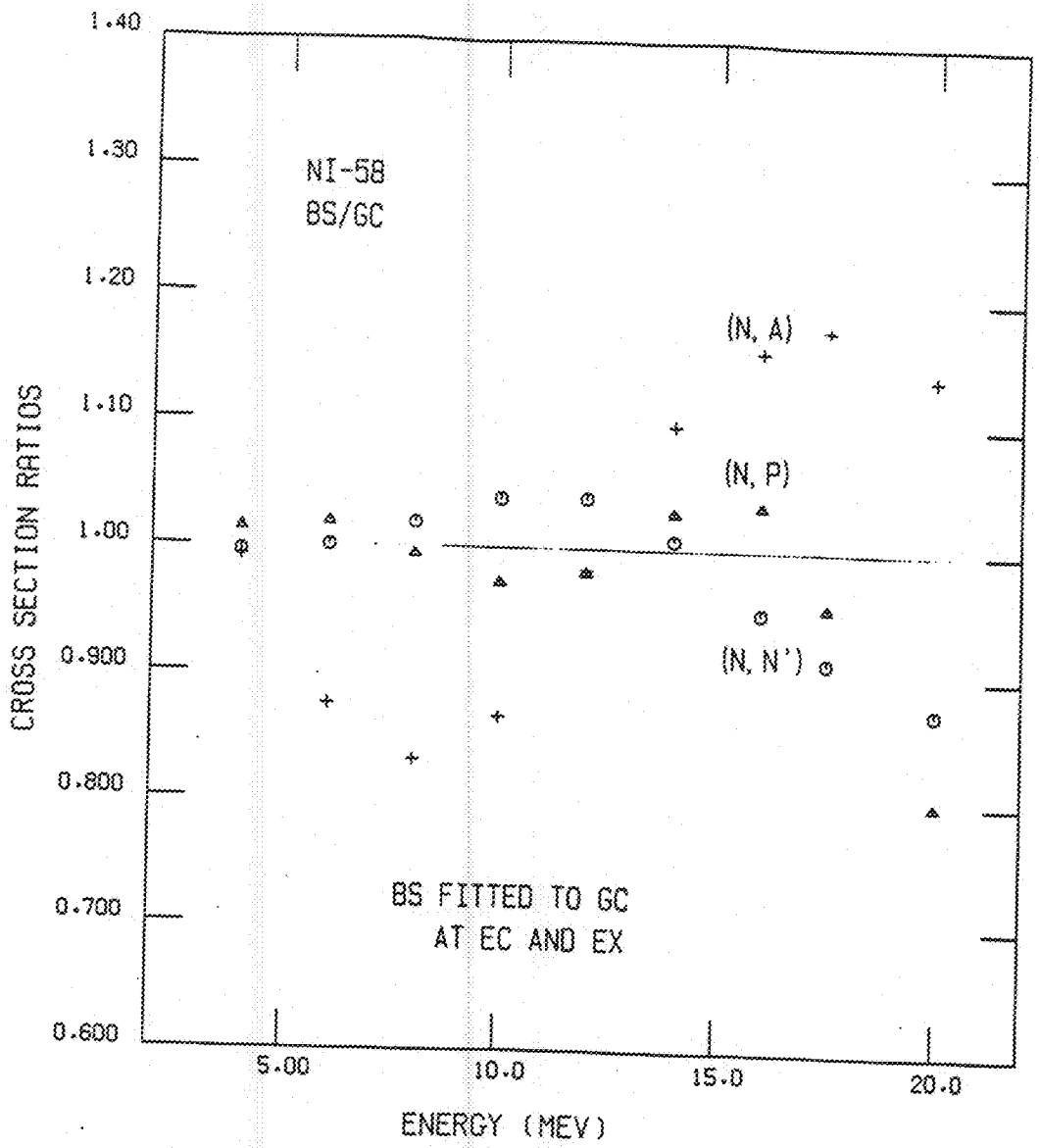

Fig. 10. The ^{58}Ni(n, n'), (n, p), and (n, α) cross sections calculated using the BSFG and G-C level densities compared in Fig. 9 are compared as ratios. The minimum in (n, α) at 8 MeV indicates that the rise-flatten-rise shape seen in Fig. 1 but not in Fig. 7 re-appears. See text for explanation.

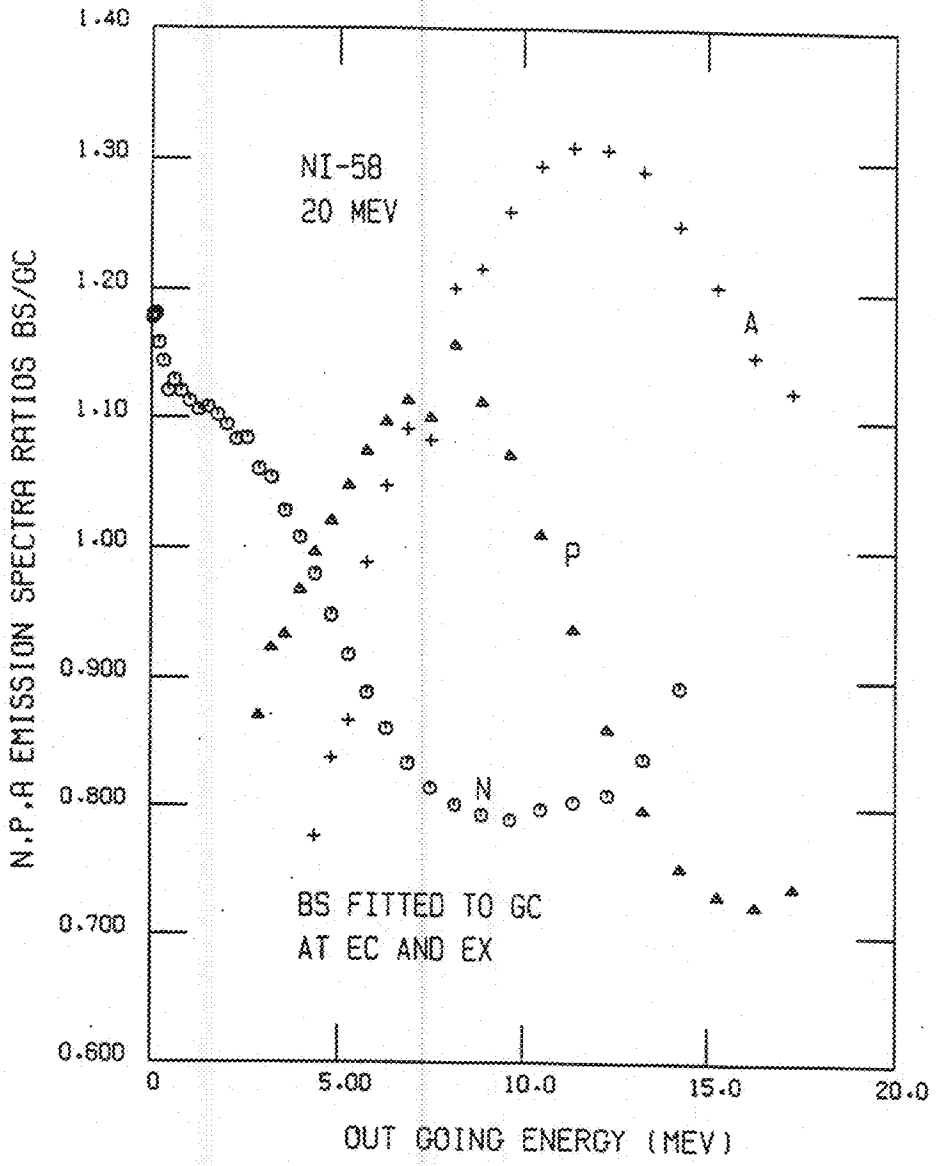

Fig. 11. Same as Fig. 6 except for a different set of level-density parameters obtained from the calculations shown in Fig. 8. The peak in the alpha-particle emission ratios is now lower because the ^{55}Fe tail shown in Fig. 9 is lower.

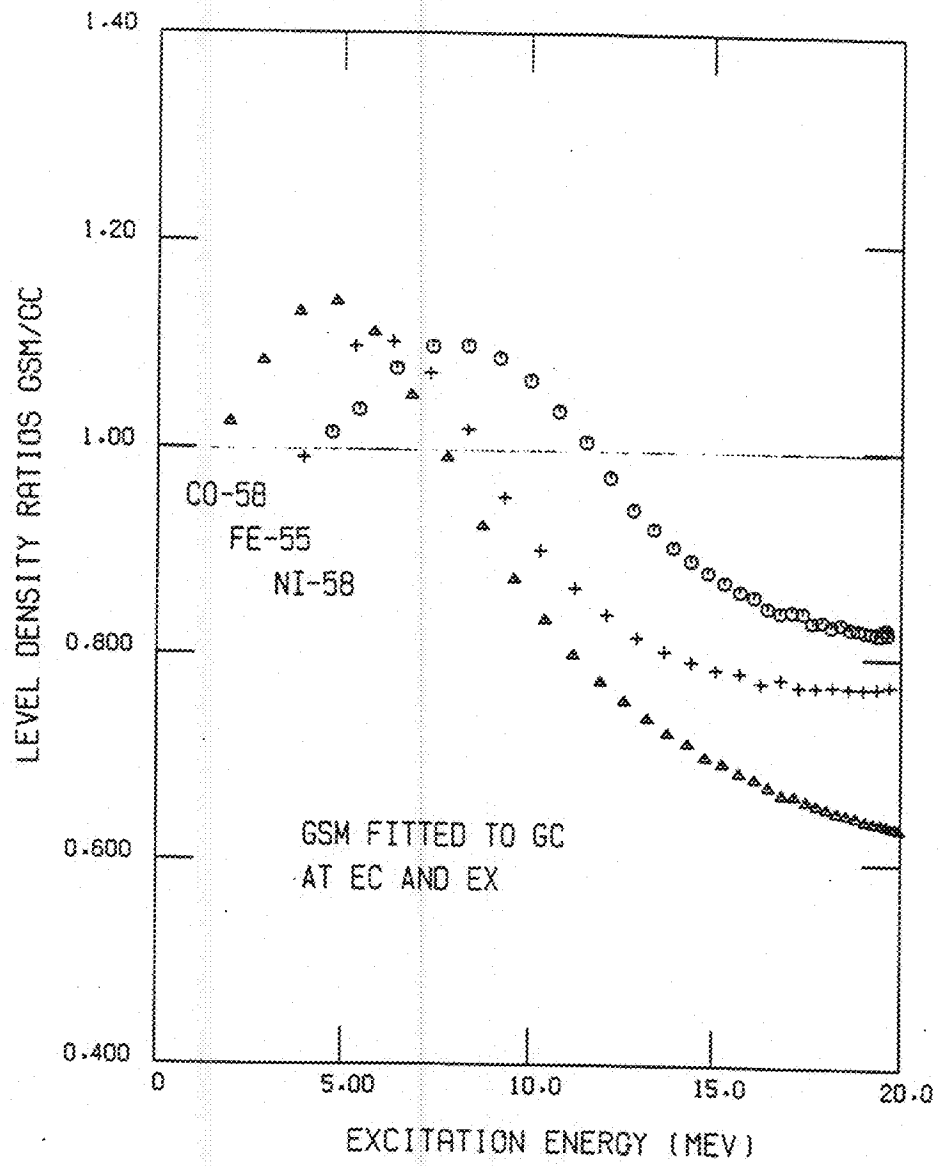

Fig. 12. Parameters of the GSM formalism are determined by fitting its level densities at two energies, E_c and E_x, to G-C used in the calculation shown in Fig. 8. The resulting level densities in GSM and G-C are compared as ratios for three residual nuclides in the binary reactions of neutrons with ^{58}Ni. Relative to the BSFG/G-C ratios shown in Fig. 9, the present ratios are closer to unity but have different shapes for the three residual nuclides.

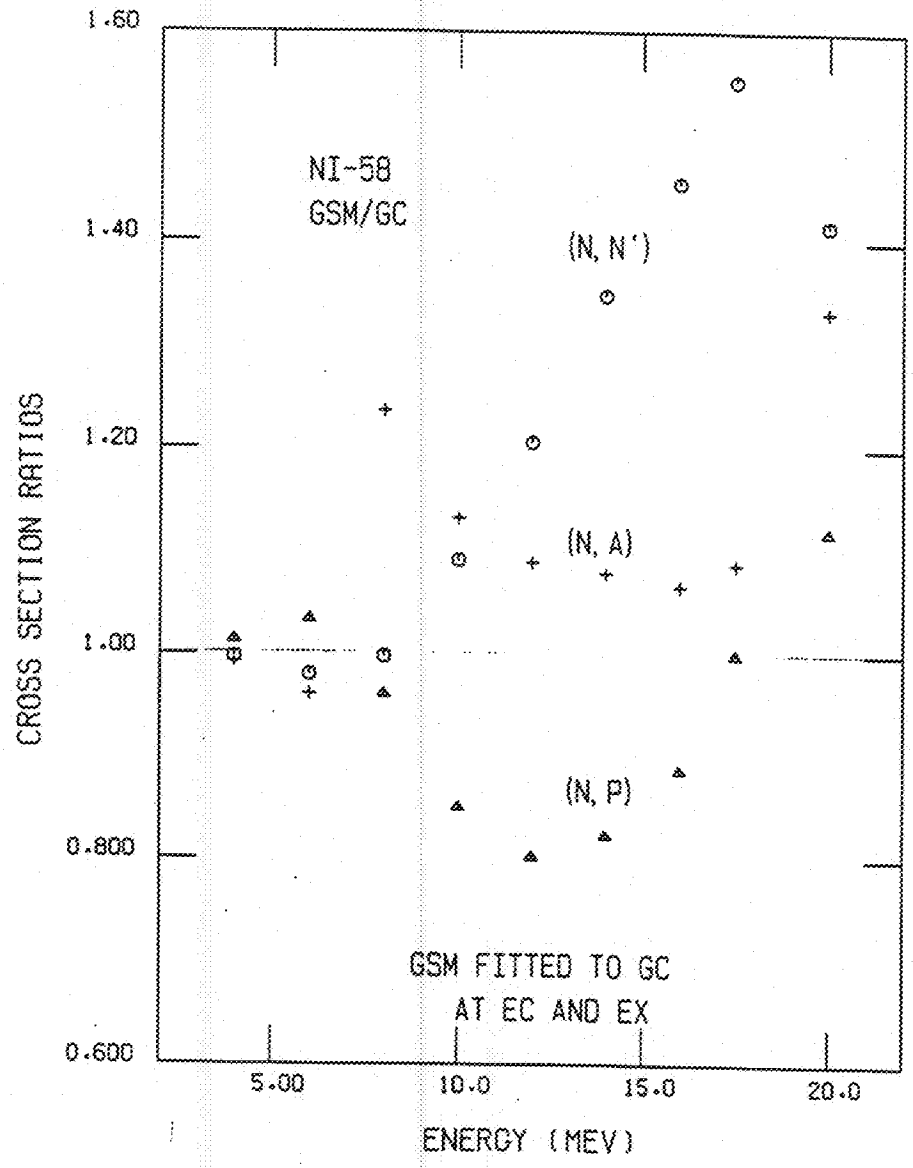

Fig. 13. The ^{58}Ni(n, n'), (n, p), and (n, α) cross sections calculated using the GSM and G-C level densities indicated in Fig. 12 are compared as ratios. Comparing with the corresponding BSFG/G-C ratios shown in Fig. 10, the (n, α) ratio at 8 MeV appears as a maximum instead of a minimum and the high-energy (n, n') ratios instead of (n, α) are larger. See text for explanation.

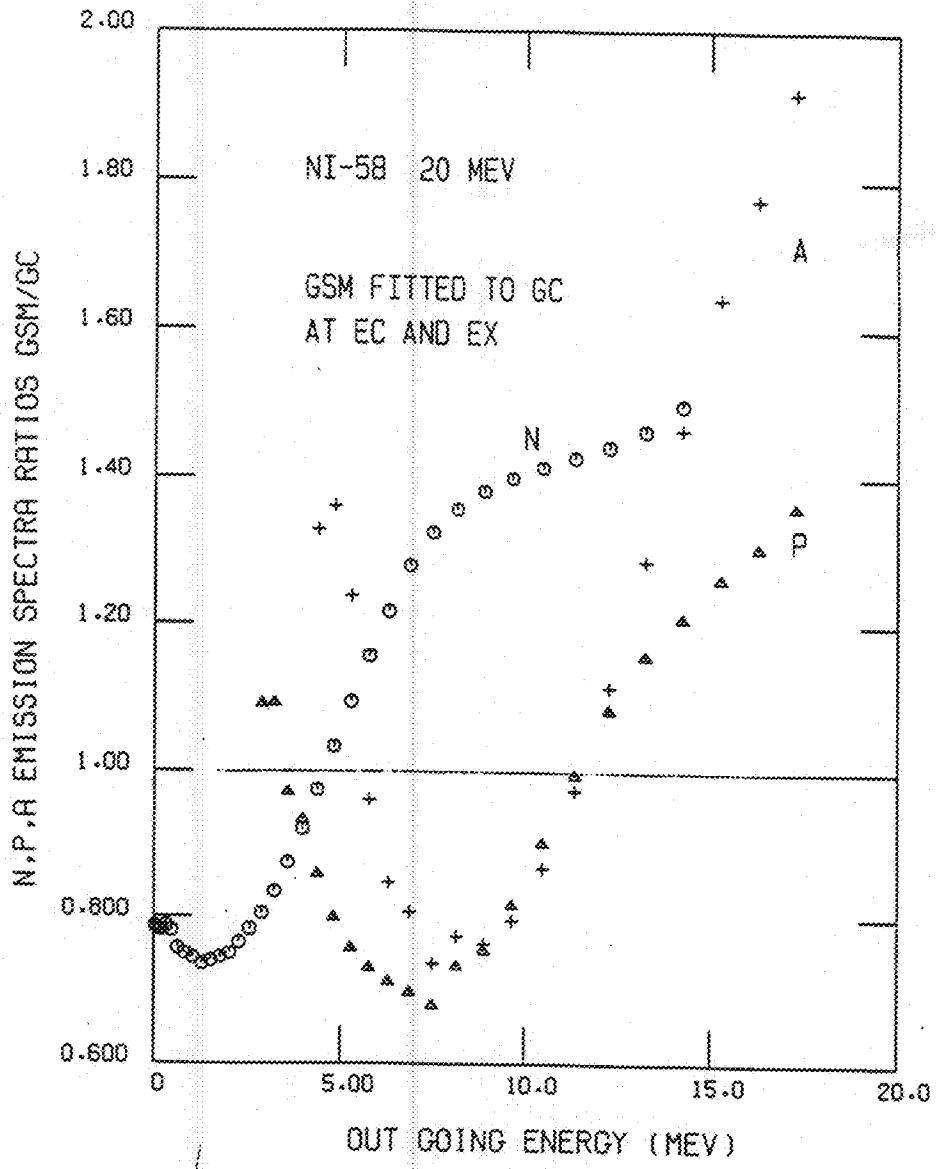

Fig. 14. Neutron, proton, and alpha-article emission spectra for an incident neutron energy of 20 MeV calculated using the GSM and G-C level densities indicated in Fig. 12 are compared as ratios. These ratios behave differently from those for BSFG/G-C shown in Fig. 11 because both the level-density ratios shown in Fig. 12 and the cross-section ratios shown in Fig. 13 have new characteristics.